

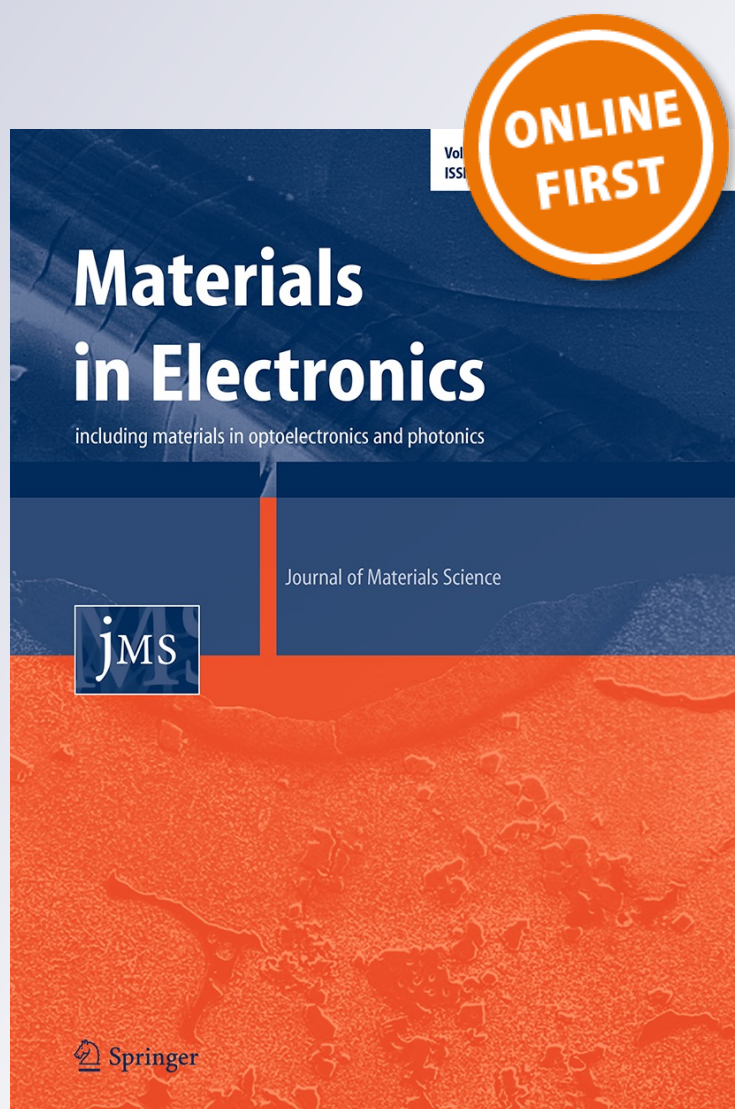
Comparative corrosion behaviour of different Sn-based solder alloys

Silvia Farina & Carina Morando

**Journal of Materials Science:
Materials in Electronics**

ISSN 0957-4522

J Mater Sci: Mater Electron
DOI 10.1007/s10854-014-2422-0



Your article is protected by copyright and all rights are held exclusively by Springer Science +Business Media New York. This e-offprint is for personal use only and shall not be self-archived in electronic repositories. If you wish to self-archive your article, please use the accepted manuscript version for posting on your own website. You may further deposit the accepted manuscript version in any repository, provided it is only made publicly available 12 months after official publication or later and provided acknowledgement is given to the original source of publication and a link is inserted to the published article on Springer's website. The link must be accompanied by the following text: "The final publication is available at link.springer.com".

Comparative corrosion behaviour of different Sn-based solder alloys

Silvia Farina · Carina Morando

Received: 21 August 2014 / Accepted: 20 October 2014
© Springer Science+Business Media New York 2014

Abstract Sn–Pb solders, particularly Sn–37 %Pb eutectic alloy, have been widely used as low temperature joining alloys for some time. However, the restriction of Pb use in industry has been strongly promoted to protect the environment and establishing a Pb-free solder has become a critical issue and an important task for material engineers. New solders must fulfil several requirements; in particular they must be corrosion resistant. In the present work, the corrosion behaviour of five Pb-free solders was studied in a 0.1 M NaCl aqueous solution by means of polarization measurements (corrosion potential measurements, potentiodynamic polarization curves and linear polarization resistance tests), and compare to that of a conventional Sn–37 %Pb solder alloy and pure Sn. The results show that the Sn–3.5 %Ag–0.9 %Cu, Sn–3.5 %Ag and Sn–0.7 %Cu solders have the best resistance to localized as well as to general corrosion, similar to that obtained for the Sn–37 %Pb solder and pure Sn. The Sn–57 %Bi solder has poorer corrosion properties but its behaviour is still acceptable, because it passivates and shows a relatively low corrosion rate. In all these cases the corrosion resistance is

good due to the content of noble elements (Ag, Cu, Pb and Bi) in the alloys. On the other hand, the Sn–9 %Zn is definitely the one that exhibits the worst behaviour, not only to localize but also to general corrosion, due to the addition of a less noble material to the Sn matrix.

1 Introduction

In the modern electronics industry, soldering is the most important technique to connecting the electronic devices and substrates. As a joining material, solder provides electrical contacts and facilitate thermal paths for heat dissipation, as well as mechanical integrity in electronic assemblies [1–3]. Sn–Pb solders, particularly Sn–37 %Pb eutectic alloys, have been widely used as low temperature joining alloys for some time due to their low cost, good solderability, low melting temperature and satisfactory mechanical properties. However, concerns about Pb toxicity have resulted in the ban of Pb-containing solders for use in water piping, food and beverage cans, and automotive applications. In the electronics industry, the main concern regarding Pb-containing solders arises from the ultimate disposal of solder-containing devices in landfills when the recycling of electronics components is not properly practiced. The restriction of Pb use in industry has been strongly promoted to protect the environment [4, 5] and establishing a lead free solder (LFS) has become a critical issue. In fact, many studies of new solders have been reported in the last decade [6]. New solders must fulfil several requirements both from economic and physical/chemical points of view. For example, the melting temperature must be in the same range as that for conventional solders (177 °C for the conventional Sn–Pb alloy), strength and integrity must be similar or superior to conventional

S. Farina (✉)
Comisión Nacional de Energía Atómica (CNEA), Comisión
Nacional de Investigaciones Científicas y Técnicas (CONICET),
Univ. de Gral. San Martín (UNSAM), Av. Gral Paz 1499 (1650),
San Martín, Argentina
e-mail: farina@cnea.gov.ar

C. Morando
Centro de Investigaciones en Física e Ingeniería del Centro de la
Provincia de Buenos Aires (CIFICEN-UNCPBA), Instituto de
Física de Materiales Tandil (IFIMAT-UNCPBA, CICPBA, MT),
Pinto 399, B7000GHG Tandil, Argentina

solders, supply must be adequate for the required uses, and prices must be competitive.

The ideal LFS alloy would be eutectic or near-eutectic, with a liquidus temperature low enough to avoid damaging components and a solidus temperature high enough to maintain joint reliability during thermomechanical fatigue. There are several candidate Sn-based alloys such as Sn–Ag, Sn–Cu, Sn–Zn, Sn–Bi. In particular, alloys of Sn–Ag–Cu (SAC alloys), have considerably attracted attention especially for automotive, industrial and electronic applications. Two of the main benefits of this system are its low melting temperature (214 °C) compared with the Sn–Ag binary eutectic alloy (218 °C) and its distinguished wetting behaviour without losing strength. Also, the SAC solder-joint electrical properties appear to be attractive for both surface-mount and ball-grid-array assembly methods. Thus, Sn–Ag–Cu alloys are considered one of the most favourable systems as a Lead-free standard alloy replacement [7–11]. However, the properties of these LFS alloys in corrosive environments have not been widely reported, though it is of importance in many automotive, aerospace, maritime and defence applications. Sn–Zn alloys are also a possible alternative for Sn–Pb solders as they cost less and show good mechanical properties. The melting temperature of the Sn–9 %Zn eutectic alloy is close to that of a Sn–Pb eutectic alloy (197 °C). However, as Zn is an active metal, the presence of this component in the alloy may decrease substantially the corrosion resistance. Finally, the eutectic Sn–57 %Bi solder (melting temperature equal to 134 °C) is already in use as replacement of the Sn–Pb eutectic solder for low temperature applications [12, 13].

Though some of these alloys are currently being used in different industries, a comparative study of their corrosion resistance is lacking. Thus, the aim of the present work is to evaluate and compare the corrosion susceptibility of different tin alloys in a unique medium, using the same techniques. To this purpose the corrosion properties of Sn–Ag, Sn–Cu, Sn–Ag–Cu, Sn–Zn and Sn–Bi solders were investigated and the results were compared with those of the eutectic Sn–Pb solder and pure Sn. These materials may undergo atmospheric corrosion in the presence of air and moisture at high temperatures [14, 15], and electrochemical corrosion in aqueous solutions containing certain acids [16, 17] or particularly aggressive species, such as chloride ions. In fact, aqueous chloride solutions are the most studied ones not only for their aggressiveness but also for being chloride one of the most abundant species in nature [17–29]. The chloride concentration in seawater corresponds to NaCl 3.5 wt%, which is approximately equal to a 0.6 M NaCl solution. Taking into account that this chloride concentration is relatively high and, in consequence, not very probable to find in practical conditions for a solder alloy, in the present work the corrosion

Table 1 Sn alloys used in the present study

Notation	Alloy composition (mass %)
T	Sn–3.5 %Ag–0.9 %Cu
A	Sn–3.5 %Ag
C	Sn–0.7 %Cu
S	Pure Sn
P	Sn–37 %Pb
B	Sn–57 %Bi
Z	Sn–9 %Zn

susceptibility of the materials was evaluated in a 0.1 M NaCl solution.

2 Experimental

To evaluate the corrosion resistance of the alloys under study, potentiodynamic polarization measurements were carried out in a conventional three-electrode cell using a saturated calomel electrode (SCE) as a reference, a platinum electrode as counter and a solder sample as the working electrode. Six different Sn alloys with Ag, Cu, Bi, Zn and Pb were prepared from pure elements. The alloys used in this study were obtained starting from 99.99 % analytical purity Sn, Ag, Cu, Zn, Bi and Pb elements. These were melted in a SiC crucible coated internally by ceramic protective coating, and heated in an electric resistance furnace under argon gas flow, cast in a graphite mold and cooled in air. The solidified samples were polished for microstructural observations. Both optical microscopy (OM) and scanning electron microscopy (SEM) were used to characterize the microstructure. Energy dispersive X-ray microanalysis (EDX) was used to characterize the compositions. Microstructural analysis was performed on metallographic specimens that were polished following standard metallographic procedures, etched with 2 % HCl in alcohol and electrolytically polished with butylcellosolve 80 cc, 10 cc glycerin and 10 cc perchloric acid. Table 1 shows the composition of each alloy and the notation used in the figures for their identification. Samples of pure Sn were also tested for comparison. An analysis of the solidification process of these alloys was carried out in a previous work [30].

Prior to each experiment the samples, 10 × 10 × 2 mm in size, were manually ground sequentially with waterproof emery paper from 220 to 600 grit, then mechanically polished using 6 μm Al₂O₃ powder followed by washing with distilled water and acetone. The surface area of the sample exposed to the test solution was 0.6 cm². All the experiments were performed in aerated 0.1 M NaCl solution at room temperature.

The samples were placed inside the cell and a stable open circuit potential was allowed to developed. This steady-state open circuit potential was obtained after a period of half an hour. Then, potentiodynamic polarization curves were recorded at a scan rate of 0.5 mV s^{-1} in the anodic direction, from a potential approximately 200 mV lower than the open circuit potential up to 0 V_{SCE} (which occurred in most cases when the current density was of the order of 10 mA cm^{-2}). Duplicate/triplicate tests were carried out with each alloy, using a new sample and fresh solution in each test.

In another set of experiments the corrosion process was followed by means of linear polarization resistance (LPR) measurements. The LPR method is based on the observation that the polarization curve close to the open circuit potential is linear, and the slope $\Delta E/\Delta I$ (ΔE being a step in potential and ΔI the resulting current change) in that region is defined as the polarization resistance, R_p . The R_p value is related to the corrosion current density (I_{corr}) by the formula:

$$I_{\text{corr}} = B/R_p$$

where B is a constant. The calculation of a corrosion rate from R_p measurements is straightforward (should the B values are known) and correct only for general corrosion attack. In these tests, the potential of the samples was varied $\pm 10 \text{ mV}$ from the open circuit potential at a 0.5 mV s^{-1} scan rate. All measurements were performed employing an Autolab PGSTAT 30 potentiostat controlled by a personal computer. SEM was used to investigate the morphology of the alloy surface after the electrochemical tests. The SEM images were compared to the OM images of the original microstructures.

3 Results and discussion

Repetitive results were obtained and representative curves are shown in this section. Figure 1 shows the evolution of the open circuit potential (E_{oc}) as a function of time for each material tested. In most cases the E_{oc} decreases quickly after immersion in the solution and, after a period of approximately half an hour, a constant value is obtained. This initial decrease of the E_{oc} can be attributed to the formation of a layer of corrosion products that finally completely covered the material surface. The Sn–Zn alloy E_{oc} slightly increases with time. Three groups of results can be identified: the Sn–Bi alloy, which is the one with the most noble E_{oc} ; the Sn–Ag, Sn–Cu, Sn–Ag–Cu and Sn–Pb alloys and the pure Sn, that show a E_{oc} of intermediate value; and the Sn–Zn alloy that shows the lowest E_{oc} . Taking into account that the higher the E_{oc} , the more noble the material from the corrosion point of view, it can be

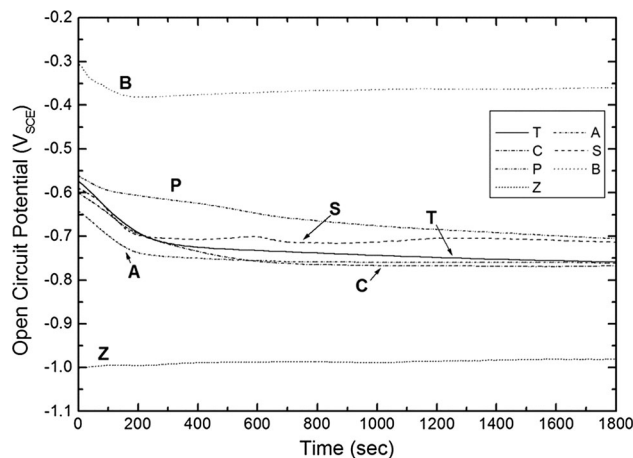


Fig. 1 Evolution of the open circuit potential as a function of time for the different alloys tested in 0.1 M NaCl solution. T: Sn–Ag–Cu; A: Sn–Ag; C: Sn–Cu; S: pure Sn; P: Sn–Pb; B: Sn–Bi; Z: Sn–Zn

concluded that the best behaviour is obtained for the Sn–Bi alloy, and the worst for the Sn–Zn alloy. An intermediate and similar behaviour is obtained for the rest of the alloys and pure Sn. However, it can be noticed that, among the materials included in the second group, the Sn–Pb alloy is more noble than the other alloys of the group.

The oxidation potentials decrease in the order $\text{Zn} > \text{Sn} > \text{Pb} > \text{Bi} > \text{Cu} > \text{Ag}$. The results of the E_{oc} measurements can be explained in terms of the galvanic series. Then, the large concentration of Bi in the Sn–Bi alloy (57 % in mass) is responsible of its high E_{oc} , compare to the Sn–Ag, Sn–Ag–Cu and Sn–Cu alloys that, even though they have noble metals in their composition (Ag and Cu), their concentration is much lower. In fact, the Sn–Ag, Sn–Ag–Cu and Sn–Cu alloys show a similar E_{oc} to pure Sn, indicating that the E_{oc} value is dominated by Sn and the small quantities of Ag and Cu are not enough to modify the E_{oc} value. In the same way, and accordingly to the oxidation potential sequence, the Pb content in the Sn–Pb alloy shifts the E_{oc} to higher values than those of Sn; and the Zn content in the Sn–Zn alloy lowers the E_{oc} with respect to that of pure Sn.

Figure 2 shows representative polarization curves for each material tested in 0.1 M NaCl solution. Such curves are characterized by the existence of a corrosion potential (E_{corr}), that is the potential value for which the current density is zero; the existence of a potential range in which the current density is relatively low (of the order of $\mu\text{A cm}^{-2}$); and the existence of a potential at which the current density increases abruptly, denoted breakdown potential (E_b). In the potential range in which the current density is low, the material dissolves at a very low rate and it is said that it is passivated. The value of this current density is known as passive current (i_{pass}). For potentials higher than E_b , the material loses its passivity and

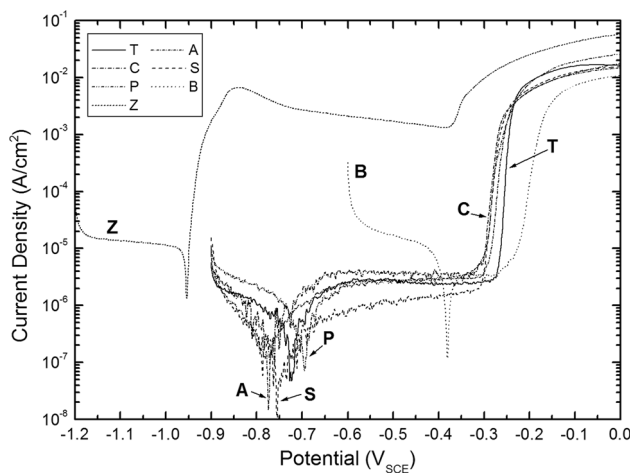


Fig. 2 Polarization curves for the different alloys tested in 0.1 M NaCl solution. *T*: Sn–Ag–Cu; *A*: Sn–Ag; *C*: Sn–Cu; *S*: pure Sn; *P*: Sn–Pb; *B*: Sn–Bi; *Z*: Sn–Zn

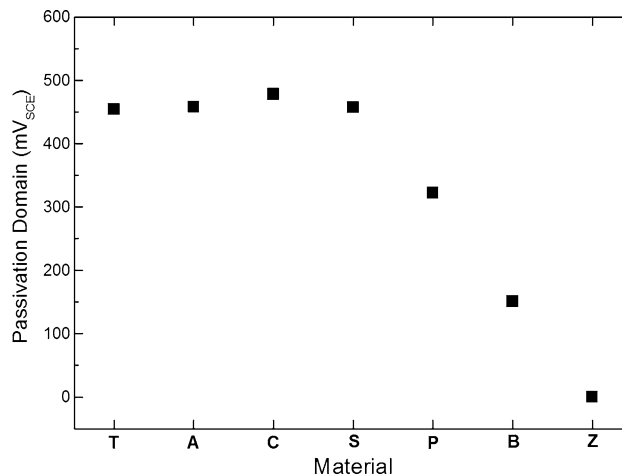


Fig. 4 Passivation domain for each of the alloys tested. *T*: Sn–Ag–Cu; *A*: Sn–Ag; *C*: Sn–Cu; *S*: pure Sn; *P*: Sn–Pb; *B*: Sn–Bi; *Z*: Sn–Zn

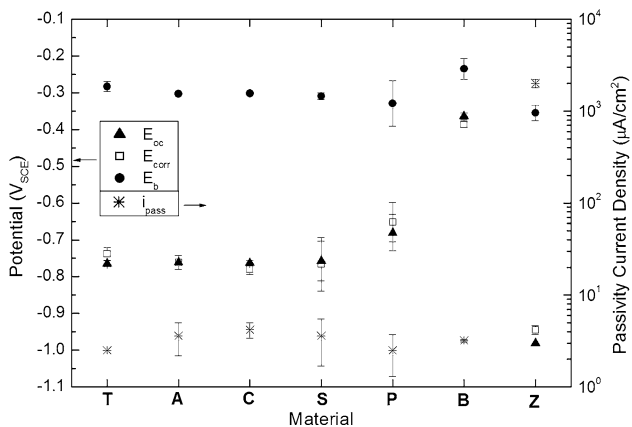


Fig. 3 Open circuit, corrosion and breakdown potentials for each of the alloys tested. Passive current densities and “pseudopassive” current density, in the case of alloy *Z*. *T*: Sn–Ag–Cu; *A*: Sn–Ag; *C*: Sn–Cu; *S*: pure Sn; *P*: Sn–Pb; *B*: Sn–Bi; *Z*: Sn–Zn

corrosion increases notably. The type of corrosion observed at potentials higher than E_b is generally localized, in the form of pits of different sizes.

Again, three groups of results can be identified. The Sn–Bi alloy is the one with the highest E_{corr} , the i_{pass} is approximately $3 \mu\text{m cm}^{-2}$ and the E_b is also the highest. A second group is composed of the Sn–Ag, Sn–Cu, Sn–Ag–Cu and Sn–Pb alloys, and pure Sn. In these cases the E_{corr} values are intermediate (from -0.78 to -0.69 V_{SCE}). The i_{pass} densities are of the order of $1\text{--}4 \mu\text{m cm}^{-2}$ and the E_b values are similar. Finally, a third group corresponds to the Sn–Zn alloy, that shows the lowest E_{corr} . In this case there is no passive region, but the current density increases abruptly when the potential is higher than E_{corr} , reaching values close to 10 mA cm^{-2} . Then, the current density

stabilizes and remains almost constant as the potential increases, showing what it could be considered as a “pseudopassivation”. However, being the current densities so high, the material undergoes an intense corrosion attack in this potential range. Then, another increase in the current density is observed, at a lower E_b than in the previous cases. In Fig. 3 the mean values of the measured parameters (E_{oc} , E_{corr} , E_b and i_{pass}) are shown for each of the alloys.

Taking into account that the most desirable situation, from the corrosion point of view, is that the E_{oc} and the E_b are as high as possible (more noble materials and difficult to be depassivated), the Sn–Bi alloy would be the one with the best corrosion resistance. However, if the difference between both potentials (E_{oc} and E_b) is considered, the Sn–Bi alloy shows a little difference compared to that of the Sn–Ag, Sn–Cu, Sn–Ag–Cu and Sn–Pb alloys, and pure Sn. The difference between E_{oc} and E_b , called passivation domain, is showed in Fig. 4. A large passivation domain is desirable, as the system is naturally at the E_{oc} and the depassivation or rupture of the passive layer may occur only if, due to some special circumstance, the potential exceeds the E_b . In this context, the Sn–Ag, Sn–Cu and Sn–Ag–Cu alloys, and pure Sn are the most corrosion resistant ones. The Sn–Pb alloy follows the sequence and the Sn–Bi alloy is even more less corrosion resistant. In the case of the Sn–Zn alloy, no passive zone is observed as the current density is high just close to the E_{corr} , and then it is the most corrosion prone one.

Finally, the resistance to a uniform type of corrosion attack was investigated through LPR measurements. Figure 5 shows the mean values and the deviation of the R_p obtained for each material. Taking into account that the higher the R_p value the lower the corrosion current density, and thus the corrosion rate, the Sn–Ag–Cu, Sn–Ag and

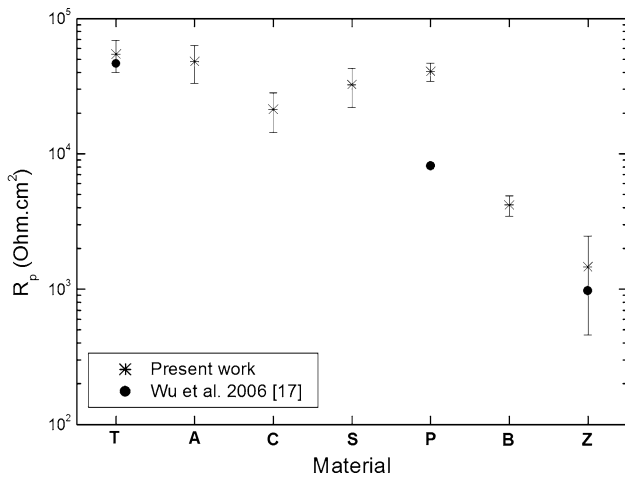


Fig. 5 Polarization resistance of each of the alloys tested in 0.1 M NaCl solution. T: Sn–Ag–Cu; A: Sn–Ag; C: Sn–Cu; S: pure Sn; P: Sn–Pb; B: Sn–Bi; Z: Sn–Zn

Sn–Pb alloys, and pure Sn are the most resistant ones. The Sn–Cu alloy is slightly less resistant, and the sequence continues with the Sn–Bi alloy and finally the Sn–Zn alloy, which is the least corrosion resistant one. Data obtained from literature [17] is also shown in the same figure for comparison. R_p values reported are similar to those obtained in the present work, though slightly lower, probably due to the fact that Wu et al. [17] used a more concentrated chloride solution (3.5 wt% NaCl).

To convert R_p values into I_{corr} values, the B value must be known. This value depends on the characteristics of the anodic and cathodic slopes in the polarization curves, and is usually in the range 10–100 mV. In fact, B values obtained from literature are found between 16 and 26 mV according to Wu et al. [17], and between 96 and 100 mV according to Mohanty et al. [21–24]. Considering the results obtained in the present work, B values were calculated assuming that the anodic parts of the polarization curves were dominated by passive behaviors, and then the B values are computed as $\beta_c/2.303$ (as β_a tends to infinite), where β_c and β_a are the corresponding cathodic and anodic Tafel slopes, respectively. In this way, B values close to 100 mV were obtained in all systems. Then, considering that B may vary from 10 to 100 mV, a minimum and a maximum I_{corr} can be estimated. Moreover, if the valence of the metallic ion is known (n), the I_{corr} in $A.cm^{-2}$ can be converted into corrosion rate (C_r) in $mm.year^{-1}$ by Faraday's Law:

$$C_r = 3,15 \times 10^8 \times I_{corr} \times M/\delta \times F \times n$$

where M is the molecular weight in $g mol^{-1}$, δ is the density in $g cm^{-3}$, and F is the Faraday's constant ($96,500 C mol^{-1}$). In this way a minimum and a maximum C_r was estimated for each material, and the results obtained

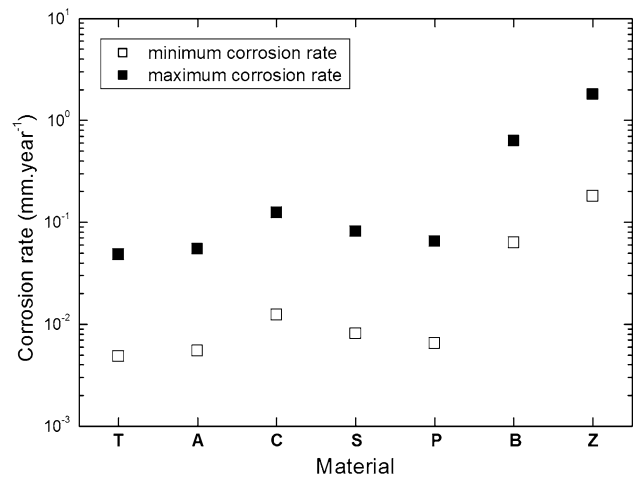


Fig. 6 Corrosion rates of the different materials tested in 0.1 M NaCl solution. T: Sn–Ag–Cu; A: Sn–Ag; C: Sn–Cu; S: pure Sn; P: Sn–Pb; B: Sn–Bi; Z: Sn–Zn

are shown in Fig. 6. The Sn–Ag–Cu, Sn–Ag, Sn–Cu and Sn–Pb alloys, and pure Sn show similar corrosion rate values of approximately 10^{-2} – $10^{-1} mm year^{-1}$. The Sn–Bi alloy shows higher corrosion rates (one order of magnitude higher), and the Sn–Zn alloy shows the highest corrosion rates (between 0.2 and 2 $mm year^{-1}$). Taking into account the use for which these alloys are developed (mostly solders in electronic devices), it could be considered that a corrosion rate of less than $0.1 mm year^{-1}$ is acceptable, while corrosion rates higher than this value should be avoided in order to guarantee the service life of components and devices. In this context, the Sn–Zn alloy is not a recommendable solder choice, the Sn–Bi alloy exhibits acceptable corrosion properties, and the Sn–Ag–Cu, Sn–Ag, Sn–Cu and Sn–Pb alloys, and pure Sn are the best ones from the corrosion point of view.

Figures 7, 8, 9, 10 and 11 show pictures of the original microstructures (Sn–Ag–Cu alloy is not shown because it is very similar to Sn–Ag or Sn–Cu alloys) and the surfaces observed by SEM after polarization in the saline solution.

The original microstructure of the Sn–Ag and Sn–Cu alloys is characterized by large dendritic Sn phase grains (bright phase) surrounded by an eutectic microstructure composed by a Sn-rich phase and intermetallic sheets of Ag_3Sn or Cu_6Sn_5 (dark phase), respectively (Figs. 7a and 8a). In both cases it can be observed that the Sn-rich phase (bright phase) corrodes selectively in the chloride solution (Figs. 7b and 8b). The intermetallic particles are nobler than the Sn-rich phase and act as cathode zones. The microstructure of the ternary eutectic Sn–Ag–Cu alloy (not shown) consists of a β -Sn phase, and a binary Sn–Ag eutectic surrounded by ternary Sn–Ag–Cu eutectic of very fine structure. Again, the Sn-rich phase corrodes selectively. The microstructure of the Sn–Pb alloy corresponds

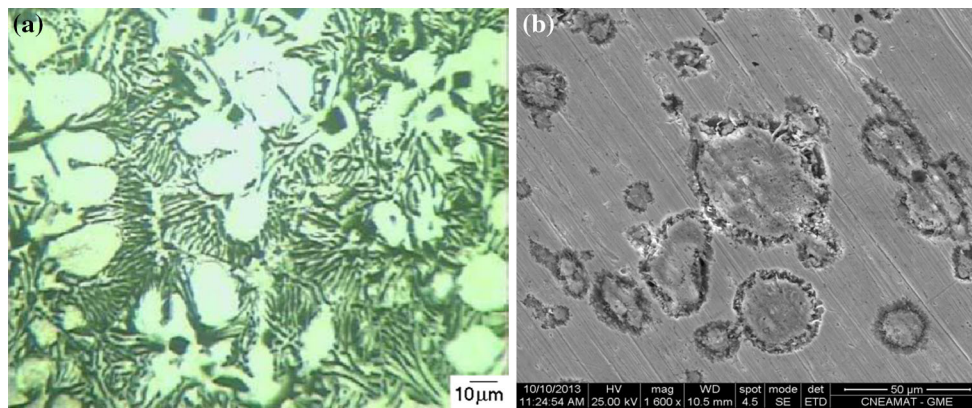


Fig. 7 Sn–Ag alloy: OM image of the original microstructure (a) and SEM image after polarization (b)

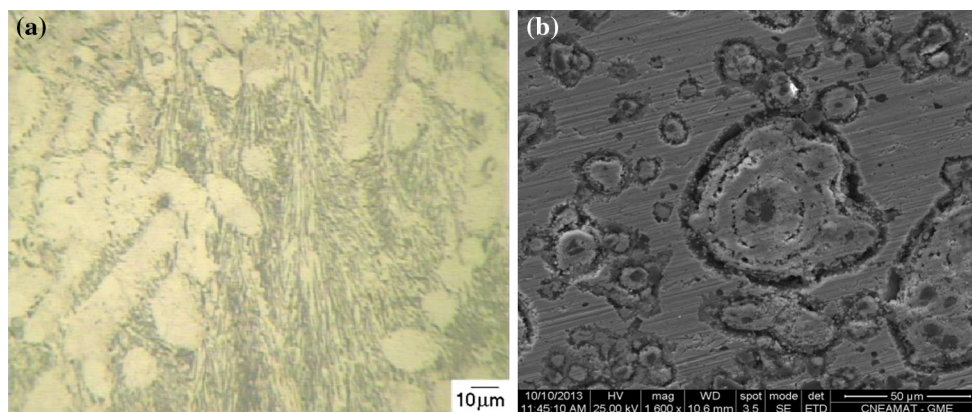


Fig. 8 Sn–Cu alloy: OM image of the original microstructure (a) and SEM image after polarization (b)

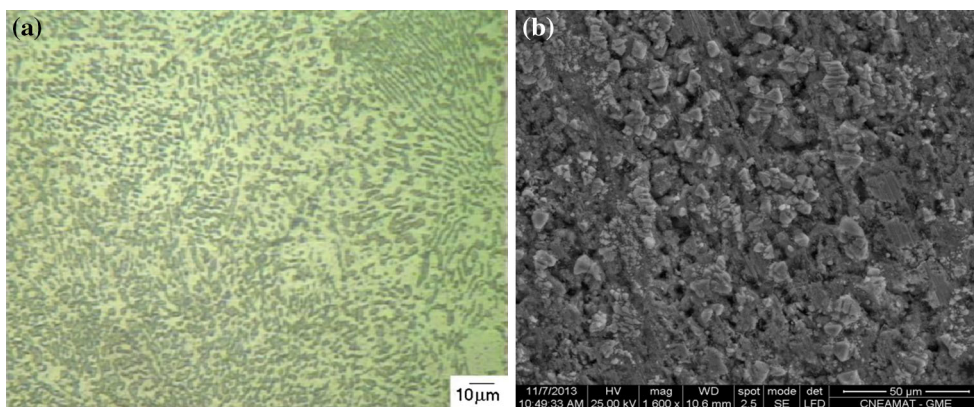


Fig. 9 Sn–Pb alloy: OM image of the original microstructure (a) and SEM image after polarization (b)

to a lamellar eutectic in which a Pb-rich phase (dark phase) and a Sn-rich phase (bright phase) coexist evenly (Fig. 9a). Again, the Sn-rich phase corrodes selectively, as Pb is nobler than Sn (Fig. 9b). The microstructure of the Sn–Bi alloy (Fig. 10a) is a mixture of Bi-rich crystals in an eutectic matrix composed of Sn (bright phase) and Bi (dark

phase). The SEM image (Fig. 10b) shows a selective attack, presumably in the Sn-rich phase that is less noble than the Bi phase. The microstructure of the Sn–Zn alloy is characterized by an acicular structure of Sn crystals with a very fine eutectic phase composed of Zn-rich and Sn-rich solid solutions (Fig. 11a). This very fine microstructure

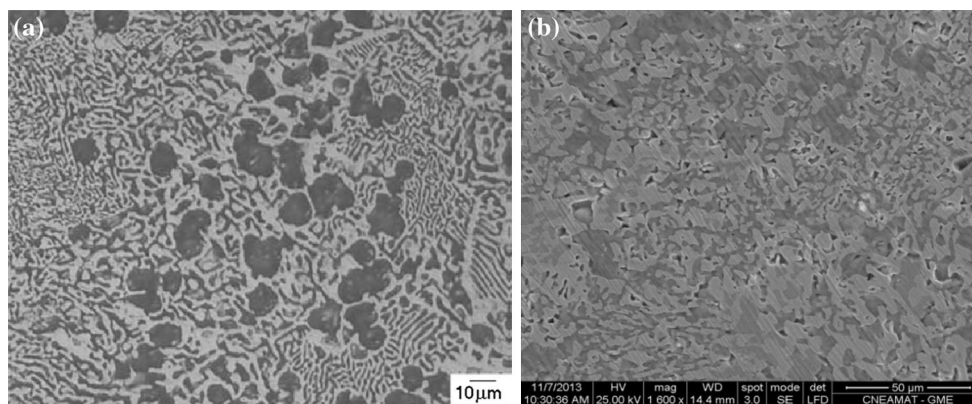


Fig. 10 Sn–Bi alloy: OM image of the original microstructure (a) and SEM image after polarization (b)

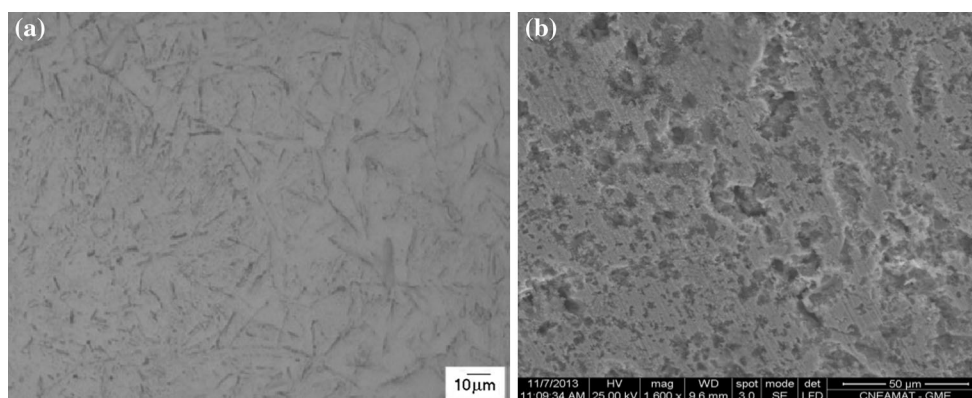
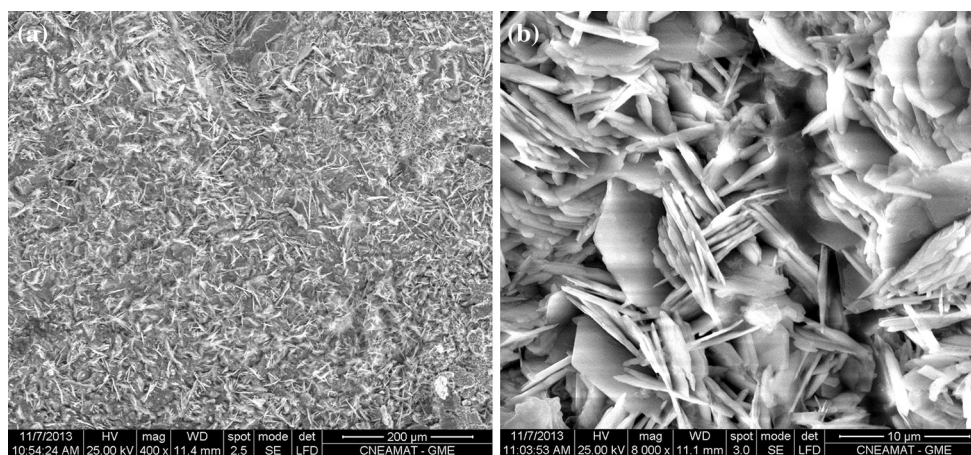


Fig. 11 Sn–Zn alloy: OM image of the original microstructure (a) and SEM image after polarization (b)

Fig. 12 SEM images of the pure Sn sample after polarization in the saline solution



seems to corrode uniformly (Fig. 11b) and this fact is consistent with the findings of Wu et al. [17] who reported that complex hydrated chlorides of Sn and Zn ($\text{Sn}_3\text{O}(\text{OH})_2\text{Cl}_2$ and $\text{Zn}_5(\text{OH})_6\text{Cl}_2\text{H}_2\text{O}$) are found on the surface.

Finally, a sample of pure Sn was polarized up to 1 V_{SCE} , allowing in this way that a thick corrosion layer developed

on the sample surface. Then, the corroded surface was observed under SEM (Fig. 12). The corrosion products found are crystals in the form of fine plates distributed on the surface with different orientations. Similar corrosion products were found by other authors [21, 24], who confirmed the presence of high amounts of Sn and Cl by EDX and assumed that the corrosion product was SnCl_2 . In

another work [22], EDX analysis revealed the presence of Sn, Cl and O in the specimen, and the authors presumed that the tin chloride formed might react with oxygen to form tin oxychlorides.

4 Conclusions

The corrosion behaviour of five Pb-free solders was studied in a saline solution by means of polarization measurements, and compared to that of a conventional Sn–Pb solder and pure Sn. The results show that the Sn–3.5 %Ag–0.9 %Cu, Sn–3.5 %Ag and Sn–0.7 %Cu solders have the best resistance to localized as well as to general corrosion, similar to that obtained for the Sn–37 %Pb solder and pure Sn (corrosion rates in the range 0.1–0.01 mm year⁻¹). Their use is possible, even in the presence of high contamination with chloride ions because corrosion rates are low (<0.1 mm year⁻¹). The Sn–57 %Bi solder has poorer corrosion properties but its behaviour is still acceptable, because it passivates and shows a relatively low corrosion rate. In all these cases the corrosion resistance is good due to the content of noble elements (Ag, Cu, Pb and Bi) in the alloys. On the other hand, the Sn–9 %Zn is found to be the one that exhibits the worst behaviour, not only to localized but also to general corrosion, due to the addition of a less noble material to the Sn matrix.

References

1. M.M. Schwartz, S. Aircraft, Welding, brazing, and soldering, Vol. 6 of ASM Metals Handbook (ASM Intl, Metals Park, Ohio, USA, 1993)
2. R. Wassink, *Soldering in electronics*, 2nd edn. (Electrochemical Publications L, Isle of Man, 1989)
3. R. Strauss, *Surface mount technology* (Butterworth-Heinemann, Oxford, 1994)
4. Directive 2002/95/EC on the restriction of the use of certain hazardous substances in electrical and electronic equipment, Official Journal of the European Union 46, 19 (2003)
5. Directive 2002/96/EC on waste electrical and electronic equipment, Official Journal of the European Union 46, 24 (2003)
6. P. Lauro, S. Kang, W. Choi, D.-Y. Shih, J. Electron. Mater. **32**, 1432 (2003)
7. S.-H. Huh, K.-S. Kim, K. Sukanuma, Mater. Trans. JIM. **42**, 739 (2001)
8. U. Kattner, JOM. **54**, 45 (2002)
9. Z. Moser, W. GÅšsior, J. PstruÅžs, S. Ishihara, X.J. Liu, I. Ohnuma, R. Kainuma, K. Ishida, Mater. Trans. JIM. **45**, 652 (2004)
10. N. Moelans, K.H. Kumar, P. Wollants, J. Alloy. Compd. **360**, 98 (2003)
11. S.W. Yoon, J.R. Soh, H.M. Lee, B.-J. Lee, Acta. Mater. **45**, 951 (1997)
12. M. McCormack, S. Jin, JOM. **45**, 36 (1993)
13. L.E. Felton, C.H. Raeder, D.B. Knorr, JOM. **45**, 28 (1993)
14. J. Jiang, J.-E. Lee, K.-S. Kim, K. Sukanuma, J. Alloy. Compd. **462**, 244 (2008)
15. M. Wang, J. Wang, H. Feng, W. Ke, Corros. Sci. **63**, 20 (2012)
16. M. Mori, K. Miura, T. Sasaki, T. Ohtsuka, Corros. Sci. **44**, 887 (2002)
17. B.Y. Wu, Y.C. Chan, M.O. Alam, J. Mater. Res. **21**, 62 (2006)
18. K.-L. Lin, T.-P. Liu, Mater. Chem. Phys. **56**, 171 (1998)
19. K.-L. Lin, F.-C. Chung, T.-P. Liu, Mater. Chem. Phys. **53**, 55 (1998)
20. H. Oulfajrite, A. Sabbar, M. Boulghallat, A. Jouaiti, R. Lbibb, A. Zrineh, Mater. Lett. **57**, 4368 (2003)
21. U.S. Mohanty, K.-L. Lin, Mater. Sci. Eng. A **406**, 34 (2005)
22. U.S. Mohanty, K.-L. Lin, Corros. Sci. **48**, 662 (2006)
23. U.S. Mohanty, K.-L. Lin, Corros. Sci. **49**, 2815 (2007)
24. U.S. Mohanty, K.-L. Lin, Corros. Sci. **50**, 2437 (2008)
25. D. Li, P.P. Conway, C. Liu, Corros. Sci. **50**, 995 (2008)
26. F. Rosalbino, E. Angelini, G. Zanicchi, R. Marazza, Mater. Chem. Phys. **109**, 386 (2008)
27. F. Rosalbino, E. Angelini, G. Zanicchi, R. Carlini, R. Marazza, Electrochim. Acta. **54**, 7231 (2009)
28. A. Ahmido, A. Sabbara, H. Zouihri, K. Dakhsic, F. Guedira, M. Serghini-Idrissi, S. El Hajjaji, Mater. Sci. Eng. B **176**, 1032 (2011)
29. W.R. Osório, L.R. Garcia, L.C. Peixoto, A. Garcia, Mater. Des. **32**, 4763 (2011)
30. C. Morando, O. Fornaro, O. Garbellini, H. Palacio, J. Mater. Sci.: Mater. Electron. (2014). doi:10.1007/s10854-014-2036-6